Online Supplement:

CaMKII causes atrial structural remodeling associated with atrial fibrillation and heart failure

Liu, Zhao PhD,[1] Finet, J Emanuel MD,[2] Wolfram, Julie A PhD,[1] Anderson, Mark E MD PhD,[3] Ai, Xun MD,[4] Donahue, J Kevin MD,[1]

From [1]the Division of Cardiology, University of Massachusetts Medical School, Worcester, MA; [2]Division of Cardiology, Cleveland Clinic Foundation, Cleveland, OH; [3]Department of Medicine, Johns Hopkins University Medical School, Baltimore, MD, and [4]Department of Physiology & Biophysics, Rush University Medical School, Chicago, IL.

Address correspondence to JKD: 55 Lake Avenue-North, University of Massachusetts, Worcester, MA 01655. (774)441-6325, donahuelab@gmail.com.

Supplemental Discussion:

Electrical remodeling in combined AF and heart failure:

The well-known association between lone AF and APD shortening is less reliably observed in heart failure. Li et al. were first to report that heart failure caused atrial remodeling in a dog model of ventricular tachypacing.[1] They noted that after 5 weeks of right ventricular tachypacing without AF, dogs had increased AF inducibility, atrial structural remodeling but in that original report they saw no change in atrial APD. In a follow-up study, the same group compared 2 weeks of atrial, ventricular and combined tachypacing.[2] They found over that shorter duration that heart failure increased atrial APD. The effects of heart failure and AF appeared to neutralize each other, with combined AF and heart failure having no change in atrial APD relative to normal controls and decreased atrial APD relative to heart failure animals. It was not clear from these 2 studies if tachypacing duration was a relevant factor or if it was just a discrepancy between the two reports. Schoonderwoerd et al. found a similar reduction in AF effects on atrial APD with 4 weeks of combined atrial and ventricular tachypacing in goats.[3]

Reported data for humans is more complex, likely due to the differences in cardiac disease severity, tissue sources, and measurement techniques between reports. Molina et al., Workman et al. and Schreieck et al. found no significant difference in atrial APD comparing heart failure patients to controls.[4-6] In contrast, Schmidt et al., Sanders et al., Fedorov et al. and Koumi et al. all found increased atrial APDs in heart failure patients compared to controls.[7-10] Of these, Schmidt and Molina studied AF in addition to heart failure, and both found that AF shortened the atrial APD. In Schmidt's case where the atrial APD was prolonged with heart failure, the APD in combined AF and heart failure was not statistically different than sinus rhythm-no heart failure controls. For Molina, where the atrial APD was unaffected by heart failure, the atrial APD in AF-heart failure was shorter than sinus rhythm-no heart failure controls.

Our pig data agree with a prior study by Lugenbeil et al showing no change in atrial APD in pigs with combined AF and heart failure.[11] In this report we show that atrial APD is not significantly different in pigs with sustained AF and heart failure relative to sinus rhythm-no heart failure controls. Pulling all of these observations together, a consistent observation is that AF shortens APD, either from a normal baseline in subjects without heart failure, or from a potentially increased value in heart failure subjects. The effects of heart failure on atrial structural remodeling appear consistent across several reports. The effects of heart failure on atrial electrophysiology are not consistent, which may be a function of the extent of heart failure (reports with more severe heart failure seem to show increased atrial APD), species differences, technical differences, or other as yet unidentified factors. Since the combined entity of AF and heart failure is so prevalent, further careful study, paying attention to these potentially confounding factors, is warranted.

Inflammatory pathways and atrial structural remodeling

It was with some surprise that we found no effect of CaMKIIn gene transfer on the atrial inflammatory cell infiltrate. We suspect that the lack of effect was due to redundancy in inflammatory drivers, so that block of a one signaling cascade is insufficient to eliminate the inflammatory pull of the multiple interconnected pathways stimulated by AF. Several inflammatory signaling pathways have been associated with AF, including the TNF-α, TGF-β, NF-κB and PPARγ pathways (for more comprehensive review, please see Hu et al.[12]). Participating cells in these inflammatory cascades include cardiac myocytes, fibroblasts, endothelial cells and inflammatory cells. In our study, gene delivery occurred at a single time point, so transduced cells would have included atrial myocytes, fibroblasts and any inflammatory cells that were present at the time of gene transfer, but recruited fibroblasts and inflammatory cells would not have been affected by our intervention. Our data suggest that even with CaMKII inhibition, sufficient signaling is still present within the atria to recruit inflammatory cells.

Recent study by Willeford et al. showed that CaMKIIδ (the relevant cardiac isoform) contributed to inflammation in a transgenic mouse model that was exposed to angiotensin II.[13] They exposed mice to angiotensin-II for between 1 hour and 3 days and found that mice with cardiac-specific deletion of CaMKIIδ had reduced NF-kB activation, inflammation and fibrosis. The differences between Willeford's model (hours to a few days angiotensin-II exposure in transgenic mice) and our model (1-2 weeks of combined, severe atrial and ventricular stress in pigs) make the results difficult to compare. The mouse model has no significant apoptosis, which is a prominent component of the AF response in our data and others. With these caveats, the Willeford results suggest that CaMKII activation is an early component in the inflammatory cascade, and our results suggest that other factors may become prominent at later timepoints overwhelming the anti-inflammatory effects of CaMKII block

A recent report by Yao et al. suggests that atrial myocyte signaling through the NLRP3 inflammasome may explain some of this inflammatory signaling.[14] Yao found that components of the NLRP3 inflammasome were increased in patients with long-standing persistent AF. They also noted increases in some but not all components of the same pathway in dogs with atrial tachypacing and CREM mice. They created a transgenic mouse line with cardiomyocyte-specific expression of NLRP3 and found among other things an increase in atrial hypertrophy and fibrosis. They observed an increase in Mef2c, and they speculated that the NLRP3-mediated inflammation and hypertrophy acted through CaMKII via the Mef2c pathway. They did not directly measure CaMKII, and others have shown that Mef2c signaling can be driven by a variety of factors, including phosphatidylinositol 3-kinase, calcineurin and protein kinases A and C among others.[15-17] The data of Yao illustrates the complexity of issues surrounding inflammation, fibrosis, apoptosis and hypertrophy. The complex interplay of these multiple signaling pathways will require extensive study with independent manipulation of the various candidates, which is beyond the scope of our report.

Supplemental Methods:

Adenovirus Vectors. Details of virus construction have been previously published.[18] The transgene insert consisted of: CMV promoter – Human CaMKIIn (CAMK2N2) – internal ribosome entry site – green fluorescent protein. Amplification of virus stock was achieved using conventional cell culture, and virus purification was performed with Adenopur columns following the manufacturer's instructions (Puresyn, King of Prussia, PA). Virus identity was confirmed by sequencing the transgene. Virus particle concentration was calculated from ultraviolet light absorbance at 260 nm and the ratio of absorbance at 260 and 280 nm. The infectious titer was determined by plaque assay. The absence of replication competent adenovirus was confirmed by lack of PCR amplification of the E1 gene. Transgene expression was confirmed by qPCR detection of CaMKIIn. The resulting virus stock was stored at -80^{o} C before use.

Painting solution. As previously described,[19] the painting solution was prepared by chilling saline solution to 4°C and gradually adding poloxamer F127 (BASF Corp, Mt Olive, NJ). The mixture was left stirring at 4°C overnight to allow the poloxamer to completely dissolve into solution. On the morning of the procedure, trypsin (250 USP units/mg, BD Diagnostics, Sparks, MD) stock solution was added to the poloxamer/saline and the resulting solution was filter sterilized using a 200 μm filter that had been chilled to 4^{o} C prior to use. Immediately before use, adenovirus stock solution was added to the trypsin/poloxamer/saline solution. The final solution included 200 mg/ml poloxamer F127, 5 mg/ml trypsin, and 1×10^{9} pfu/ml of the virus Ad-CaMKIIn. Immediately before painting, the solution was warmed at 37°C to achieve a firm gel consistency.

Experimental protocol. All animals received humane care in compliance with the NIH's *Guide for the Care and Use of Laboratory Animals.* The protocols were approved by the Institutional Animal Care and Use Committee. A total of 35 Yorkshire pigs (weight, 25 – 30 kg) were divided into three groups:

(a) 7-day sinus rhythm, (b) 7-day AF and (c) 14-day AF (Figure 1A). Animals were randomized within groups to no virus control and AdCaMKIIn gene painting subgroups, with 5 animals per time point per subgroup. In the 14-day group, an additional subgroup named AFPC (n=5) with gene transfer of Ad-CaMKIIn and an equivalent level of AF or pacing as control was added at the end of the study. The AFPC animals were not randomized.

Each animal underwent an initial procedure that included echocardiogram, electrophysiology study, and epicardial painting of the virus/poloxamer/trypsin solution. For the AF animals, an atrial pacemaker was implanted at the initial procedure, and the pacemaker was activated immediately after the procedure to deliver burst pacing at 42 Hz frequency with a continuous 2 second on/off duty cycle. Animals were monitored on a daily basis with rhythm assessment. On post-operative day 7 or day 14, animals underwent electrophysiology study, echocardiography, and cardiac extraction for histology and molecular analysis. At the termination study, animals in AF were cardioverted at least 30 minutes before any data collection. The 7-day AF animals were used to assess structural remodeling, molecular and electrophysiological properties at peak gene effect. The 14-day animals were sacrificed after gene expression began to wane but in a time frame when structural remodeling is better established.

Pacemaker implantation and gene delivery. After sedation (telazol 1.5 mg/kg IM, ketamine 1.5 mg/kg IM and xylazine 1.5 mg/kg IM), and induction of anesthesia (isoflurane 0.5% to 1.5%), an echocardiogram was performed. The surgical site was prepared and draped in sterile fashion, and the right external jugular vein was accessed by cut-down. The chest was opened by median sternotomy and the pericardium was incised. An invasive electrophysiology (EP) study was performed as described below in detail. After EP study, 5 ml of the painting solution was painted on both atria using a painting brush. All epicardial surfaces were exposed by manipulating the heart. Each painting area was coated twice for 60 seconds each, and 60 seconds were given between painting coats in a pattern of alternating

60-second left and right atria painting for twice. After painting, the heart was exposed to air for 10 minutes to permit virus penetration.

For pacemaker implantation, an active-fixation lead was placed through the right external jugular vein into in the right atrial myocardium using fluoroscopic guidance. Successful lead placement was confirmed by assessment of electrogram size and pacing threshold of the implanted lead. The pacing lead was connected to a Medtronic stimulator (Itrel-3), which was placed in a subcutaneous pocket in the neck. The chest and neck incisions were closed, and the isoflurane anesthesia was discontinued. When the animal was recovering from anesthesia, the pacemaker was programmed to burst pace at 42-Hz frequency and 7.5-V output for 2-second increments that alternated with 2-second pauses. The only exception was for the AFPC group, which underwent an adjusted pacing protocol so that the amount of burst pacing in the AFPC group was equal to the amount of burst pacing and AF in the AF-control group (Supplement Figure 1).

Echocardiogram. At the time of gene transfer and at the termination study, animals underwent echocardiogram using a Sonos 550 Ultrasound System (Hewlett-Packard, Andover, MA) equipped with a 1.5-MHz probe (Acuson, Siemens, Malvern, PA). At the termination study, animals in AF were cardioverted at least 30 minutes before echocardiogram. Left atrial and left ventricular end-diastolic diameters and ejection fractions were measured from 2-chamber and 4-chamber images of the heart using machine-loaded software.

Left ventricular end-diastolic diameter was measured from the apical 4-chamber view basal to the insertion of the papillary muscles for consistent location. Left ventricular ejection fraction was measured using end-diastolic and end-systolic views by tracing the endocardium in each view and using the machine-loaded software to calculate ejection fraction.

Left atrial end-diastolic diameter was measured from the short axis view where it was visualized posterior and left of the aortic valve. Left atrial ejection fraction was measured in apical 2- and 4-chamber views tilted to visualize the appendage. Left atrial ejection fraction was measured using end-diastolic and end-systolic views by tracing the endocardium in each view and using the machine-loaded software to calculate ejection fraction.

Electrophysiology (EP) study. EP study was performed at the initial and termination procedures as described elsewhere.[20, 21] All data were recorded during sinus rhythm or constant rate pacing. At the termination procedure, any animals in AF were cardioverted to SR at least 30 minutes before EP study. A conventional 12-lead ECG was recorded with standard positions. Monophasic action potential (MAP) recordings were acquired with a 7-French MAP catheter (Boston Scientific, Natick, MA) positioned at the center of 10 pre-designated epicardial atrial regions and in the basal region of the ventricles, adjacent to atrial sites 4 and 9 as reported previously.[19] MAP duration was measured as the interval from the steepest part of the MAP upstroke to the level of 90% repolarization ($MAPD_{90}$) during regular pacing with a drive-train cycle length of 400 ms.

Intra-atrial conduction time was measured by pacing at 400 ms cycle length from a catheter placed at the anterior junction of the superior vena cava and the right atrium—the approximate position of the sinus node (SN), and measurement of conduction time at the tip of the left atrial appendage (LAA). The physical distance between catheters was measured by aligning surgical sutures closely on the heart surface at gene transfer and termination study to calculate conduction velocity from SN to LAA.

Rhythm. The daily electrocardiogram (ECG) was recorded with a 4-lead telemetry system on a strip as described.[20] All the groups of animals received 2-3 minute daily recordings (60 assessable 2 second off-pacing segments) except that the AFPC group received 2-5 minutes of recording due to the adjusted

pacing protocol. Animals were awake and alert at consistent levels from one recording to the next. Three investigators (ZL, JEF and JKD) blinded to study group assessed rhythm during the off-pacing segments. We defined SR as the presence of any sinus beats during the off-pacing segments and AF as the absence of organized sinus beats through a 2-second segment. Sustained AF was defined as the absence of sinus beats through the whole recording.

Histology. Atrial tissue samples were fixed with 10% formalin, embedded into paraffin, cut to 5-μm thickness sections. Hematoxylin and eosin (H&E) staining was for evaluation of nuclear and cellular size, inflammation and myolysis. H&E stained samples were examined at 400x magnification by the light microscope (Nikon Eclipse TE 2000-S, Nikon). In each atrium, 7-10 random microscope areas were selected. For nuclear and cell size measurements, images were taken from each of these areas and 7-10 cardiac muscle cells and their corresponding nuclei were randomly selected in each image. Of note, only cross-sectional-cut cardiomyocytes were selected for quantification to ensure consistency. For inflammation and myolysis, a grade was assigned by each reviewer for these measures based on our previously published criteria (Supplement Figure 6).[22, 23]

Masson's trichrome stain was used to identify the percentage of myocardial tissue area that was fibrotic. Masson's trichrome stained samples were assessed at 100x magnification. Seven random fields of views were selected from each slide. The amount of fibrosis % was defined as the areas of fibrosis divided by total tissue area. Atrial fibrosis, including interstitial and perivascular fibrosis, was selected for the analysis with an exclusion of the pericardial fibrosis/adhesion region that was present in all post-surgical specimens.

Image processing. The quantification of nucleus/cellular areas and atrial fibrosis % were achieved using custom-developed semi-automated image processing algorithms based on MATLAB 2015a (MathWorks Inc. Natick, MA) validated and assisted by manual analysis using ImageJ (NIH, Bethesda,

MD). The processing methods are shown graphically in Supplement Figures 7 and 8. The investigator performing the analysis (ZL) was blinded to animal study group identity. Prior to data analysis, the semi-automatic analysis protocols were validated by comparison to manual results from 3 observers in a blinded fashion using ImageJ software and no statistically significant difference existed between the automated methods and average results from the manual image analysis methods.

Nuclear and cell size quantification: the H&E stained images were firstly pre-processed for uneven illumination correction, intensity adjustment and contrast enhancement. In typical H&E images, the nucleus was stained blue and the cytoplasm was stained red. The global intensity thresholds were calculated to separate nucleus, cell cytoplasm and backgrounds. Nuclei and cells on the edges of the images were cleared and artifact was removed to obtain the contours of nucleus and cytoplasm. Watershed algorithm was applied to separate adjacent nuclei and cells.[24-26] After segmentation, the centroids of nucleus-cell pairs were numbered. From all the pairs, we randomly selected 7-10 nucleus/cell pairs in cross-section cut and quantified nuclear and total cellular areas.

Fibrosis% quantification: the Masson's trichrome staining images were converted from RGB space to L*a*b color space where the colors were classified using Kmeans clustering algorithm to separate fibrosis (stained blue), myocardium (stained red) and artifact (stained white) as described.[27, 28] Epicardial fibrosis was excluded by a series of steps including dilation, erosion and subtraction of the images.

Terminal deoxynucleotidyl transferase mediated biotinylated UTP nick end labeling (TUNEL) labeling. Cell apoptosis was examined by the standard TUNEL assay using TACS 2 TdT in situ apoptosis detection KIT-DAB/Fluor from R&D Systems (4812-30-K, Trevigen, MD) following the protocols by the manufacturer. The investigator performing the analysis (ZL) was blinded to study group identity at the time of the analysis. After rinsing with PBS, the slide was mounted with the ProLong

Gold Antifade Reagent (Molecular Probes, OR) to stain the entire nucleus in DAPI, and a coverslip was attached. 7-20 microscope fields were randomly selected depending on the sizes of tissue specimen (200x magnification) and approximately 500 myocytes were included in each section. All images were taken at the same microscope settings to ensure consistency. The TUNEL and DAPI images were merged to calculate TUNEL-positive index which is equal to the number of TUNEL positive nucleus divided by the total number of nucleus and multiplying 100%.

Quantitative Polymerase Chain Reaction. Flash frozen tissue samples were kept at -80° C. Total RNA was extracted by RNeasy-Mini Kit (Qiagen), and reverse transcription used the Superscript first strand synthesis system (Invitrogen). After reverse transcription, the amount of cDNA was adjusted to 10ng, and quantitative PCR was performed in triplicate using the Taqman method (PE Applied BioSystems), with an ABIprism 7900HT (PE Applied BioSystems) and commercially available Taqman primers for CAMK2N2 (Applied BioSystems assay ID Hs00536421_m1) and GAPDH (Applied BioSystems assay ID Hs02758991_g1). We used the delta-delta-Ct method for quantification and normalized CAMK2N2 gene expression to GAPDH expression.

Western Blot. Immediately after cardiac extraction, cardiac tissues were frozen in liquid nitrogen and stored at -80^{o} C. Protein was physically dissociated and homogenized in Tissue Lysis Buffer (Promega, Madison, WI) containing 1% protease and phosphatase inhibitors (Promega) for 2 x 2 minutes at 30 Hz using a Tissuelyser II (Qiagen, US). Samples were centrifuged at 12,000 rpm for 15 minutes at 4^{o} C to isolate the membrane fraction. Protein concentrations were determined by the BCA protein assay (Thermo Scientific, Rockford, IL) on a spectrophotometer. The lysates containing approximately 20 µg of protein were subjected to electrophoresis on 4-12% Bis-Tris gels (Bio-Rad, Hercules, CA), transferred to nitrocellulose membranes, blocked with 5% BSA, and probed at 4^{o}C over night with rabbit anti-CaMKII antibody (1: 1000, Ab181052, Abcam, Cambridge, MA), rabbit anti-T286-

phosphorylated-CaMKII (1:1000, Ab32678, Abcam), rabbit anti-m281/282-oxidized-CaMKII (1:1000, supplied by Mark Anderson) [29], rabbit anti-HDAC4 (1:200, sc11418, Santa Cruz Biotechnology, Santa Cruz, California), rabbit anti-S632-phosphorylated-HDAC4 (1:1000, Ab39408, Abcam), rabbit anti-p38 MAP Kinase (1:1000, cs9212, Cell Signaling Technologies, Danvers, MA), rabbit anti-Thr180/Thr182-phosphorylated-p38 MAP Kinase (1:1000, cs9211, Cell Signaling Technologies), rabbit anti-ERK 1/2 (1:1000, cs9102, Cell Signaling Technologies), rabbit anti-Thr202/Thr204-phosphorylated-ERK 1/2 (1:1000, cs9101, Cell Signaling Technologies), rabbit anti-JNK (1:1000, AF1387, R&D Systems), mouse anti-phosphorylated-JNK(1:500, sc6254, Santa Cruz), and rabbit anti-beta actin (1:3000, Ab8227, Abcam) as control protein. Membranes were then incubated with secondary anti-rabbit (1:4000, sc2004, Santa Cruz) or anti-mouse (1:2000, sc2005, Santa Cruz) IgG antibodies. Separate blots were run for SR, 7-day AF and 14-day AF animals, and the comparisons reported for SR vs. 7-day AF vs. 14-day AF were performed using the normalized expression levels of the control animals across these 3 gels. Different blots were used for each protein of interest, except that the HDAC4 and p-HDAC4 blots from the 7-day AF animals were both performed on the same blot. The protein of interest and the loading control protein (β-actin) were always measured from the same blot. For each protein, all blots from all groups were run at the same time using the same materials. For consistency, β-actin was used as the loading control protein for all blots. If these two proteins overlapped, the protein of interest was interrogated first, and then the membranes were stripped with stripping buffer (Prod #21059, Thermo Scientific) at 40 ^{o} C for 30 minutes before reprobing for β-actin. Immunoreactive bands were visualized with the western blotting luminol reagent (sc-2048, Santa Cruz). The Western blot images were scanned digitally with the Amersham Imager 600 (GE Healthcare Life Sciences) and optical density was quantified by ImageJ software.

Statistical analysis. For cardiac rhythm, echocardiography and histology analyses, the investigators performing the analyses were blinded to animal study group. For rhythm analysis, the SR percentage equals to the number of non-pacing segments with SR divided by the total number of non-pacing segments on daily telemetry recordings. The AF/burst-pacing burden was calculated as the combined time of AF and pacing divided by the total ECG recording time. They were analyzed by Poisson regression with a generalized estimating equations model to address animal-level clustering. In comparisons between multiple subgroups (SR vs. 7- and 14-day AF controls, or 14-day AF subgroups), one-way analysis of variance (ANOVA) was used with post-hoc Tukey testing between specified subgroups. Data were presented as mean ± S.E.M. Owing to non-normality distribution, the 7-day SR and AF Western blot analyses were compared with non-parametric Mann–Whitney U test. Statistical analysis was performed using SPSS Statistics. All statistical tests were conducted at the significance level of $p<0.05$.

Supplement References:

1. Li D, Fareh S, Leung T, Nattel S. Promotion of atrial fibrillation by heart failure in dogs: atrial remodeling of a different sort. Circulation 1999;100:87-95.

2. Cha TJ, Ehrlich JR, Zhang L, Shi YF, Tardif JC, Leung TK, Nattel S. Dissociation between ionic remodeling and ability to sustain atrial fibrillation during recovery from experimental congestive heart failure. Circulation 2004;109:412-418.

3. Schoonderwoerd BA, Van Gelder IC, van Veldhuisen DJ, Tieleman RG, Grandjean JG, Bel KJ, Allessie MA, Crijns HJ. Electrical remodeling and atrial dilation during atrial tachycardia are influenced by ventricular rate: role of developing tachycardiomyopathy. J Cardiovasc Electrophysiol 2001;12:1404-1410.

4. Molina CE, Abu-Taha IH, Wang Q, Rosello-Diez E, Kamler M, Nattel S, Ravens U, Wehrens XHT, Hove-Madsen L, Heijman J, Dobrev D. Profibrotic, Electrical, and Calcium-Handling Remodeling of the Atria in Heart Failure Patients With and Without Atrial Fibrillation. Front Physiol 2018;9:1383.

5. Workman AJ, Pau D, Redpath CJ, Marshall GE, Russell JA, Norrie J, Kane KA, Rankin AC. Atrial cellular electrophysiological changes in patients with ventricular dysfunction may predispose to AF. Heart Rhythm 2009;6:445-451.

6. Schreieck J, Wang Y, Overbeck M, Schomig A, Schmitt C. Altered transient outward current in human atrial myocytes of patients with reduced left ventricular function. J Cardiovasc Electrophysiol 2000;11:180-192.

7. Schmidt C, Wiedmann F, Zhou XB, et al. Inverse remodelling of K2P3.1 K+ channel expression and action potential duration in left ventricular dysfunction and atrial fibrillation: implications for patient-specific antiarrhythmic drug therapy. Eur Heart J 2017;38:1764-1774.

8. Sanders P, Morton JB, Davidson NC, Spence SJ, Vohra JK, Sparks PB, Kalman JM. Electrical remodeling of the atria in congestive heart failure: electrophysiological and electroanatomic mapping in humans. Circulation 2003;108:1461-1468.

9. Fedorov VV, Glukhov AV, Ambrosi CM, Kostecki G, Chang R, Janks D, Schuessler RB, Moazami N, Nichols CG, Efimov IR. Effects of KATP channel openers diazoxide and pinacidil in coronary-perfused atria and ventricles from failing and non-failing human hearts. J Mol Cell Cardiol 2011;51:215-225.

10. Koumi S, Arentzen CE, Backer CL, Wasserstrom JA. Alterations in muscarinic K+ channel response to acetylcholine and to G protein-mediated activation in atrial myocytes isolated from failing human hearts. Circulation 1994;90:2213-2224.

11. Lugenbiel P, Wenz F, Govorov K, Schweizer PA, Katus HA, Thomas D. Atrial fibrillation complicated by heart failure induces distinct remodeling of calcium cycling proteins. PLoS One 2015;10:e0116395.

12. Hu YF, Chen YJ, Lin YJ, Chen SA. Inflammation and the pathogenesis of atrial fibrillation. Nat Rev Cardiol 2015;12:230-243.

13. Willeford A, Suetomi T, Nickle A, Hoffman HM, Miyamoto S, Heller Brown J. CaMKIIdelta-mediated inflammatory gene expression and inflammasome activation in cardiomyocytes initiate inflammation and induce fibrosis. JCI Insight 2018;3.

14. Yao C, Veleva T, Scott L, Jr., et al. Enhanced Cardiomyocyte NLRP3 Inflammasome Signaling Promotes Atrial Fibrillation. Circulation 2018;138:2227-2242.

15. Munoz JP, Collao A, Chiong M, Maldonado C, Adasme T, Carrasco L, Ocaranza P, Bravo R, Gonzalez L, Diaz-Araya G, Hidalgo C, Lavandero S. The transcription factor MEF2C mediates

cardiomyocyte hypertrophy induced by IGF-1 signaling. Biochem Biophys Res Commun 2009;388:155-160.

16. Diaz-Meco MT, Moscat J. MEK5, a new target of the atypical protein kinase C isoforms in mitogenic signaling. Mol Cell Biol 2001;21:1218-1227.

17. Maiti D, Xu Z, Duh EJ. Vascular endothelial growth factor induces MEF2C and MEF2-dependent activity in endothelial cells. Invest Ophthalmol Vis Sci 2008;49:3640-3648.

18. Swaminathan PD, Purohit A, Soni S, et al. Oxidized CaMKII causes cardiac sinus node dysfunction in mice. J Clin Invest 2011;121:3277-3288.

19. Kikuchi K, McDonald AD, Sasano T, Donahue JK. Targeted modification of atrial electrophysiology by homogeneous transmural atrial gene transfer. Circulation 2005;111:264-270.

20. Amit G, Kikuchi K, Greener ID, Yang L, Novack V, Donahue JK. Selective molecular potassium channel blockade prevents atrial fibrillation. Circulation 2010;121:2263-2270.

21. Igarashi T, Finet JE, Takeuchi A, Fujino Y, Strom M, Greener ID, Rosenbaum DS, Donahue JK. Connexin gene transfer preserves conduction velocity and prevents atrial fibrillation. Circulation 2012;125:216-225.

22. Bauer A, McDonald AD, Nasir K, Peller L, Rade JJ, Miller JM, Heldman AW, Donahue JK. Inhibitory G protein overexpression provides physiologically relevant heart rate control in persistent atrial fibrillation. Circulation 2004;110:3115-3120.

23. Bauer A, McDonald AD, Donahue JK. Pathophysiological findings in a model of persistent atrial fibrillation and severe congestive heart failure. Cardiovascular Research 2004;61:764-770.

24. Meyer F. Topographic distance and watershed lines. Signal Process 1994;38:113-125.

25. Malpica N, de Solorzano CO, Vaquero JJ, Santos A, Vallcorba I, Garcia-Sagredo JM, del Pozo F. Applying watershed algorithms to the segmentation of clustered nuclei. Cytometry 1997;28:289-297.

26. Eddins S. Steve on Image Processing. Mathworks 2006. Available at: http://blogs.mathworks.com/steve/2006/06/02/cell-segmentation/. Accessed August 25, 2016.

27. Lloyd S. Least squares quantization in PCM. IEEE Trans Inf Theor 2006;28:129-137.

28. MathWorks. Color based segmentation using k means clustering. Available at: http://www.mathworks.com/help/images/examples/color-based-segmentation-using-k-means-clustering.html, Accessed August 25, 2016.

29. Erickson JR, Joiner MLA, Guan X, et al. A dynamic pathway for calcium-independent activation of CaMKII by methionine oxidation. Cell 2008;133:462-474.

Supplement Figure 1: AFPC group

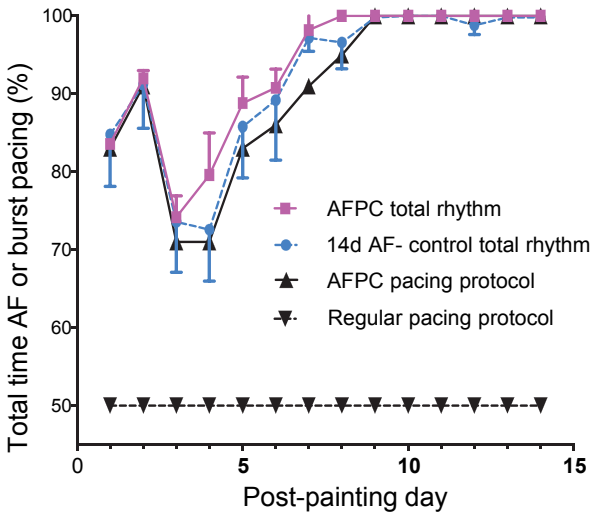

AFPC adjusted burst pacing protocol

day	14d AF control (target data):		AFPC burst pacing cycle		
	measured SR% (of 50% non-burst pacing time)	Total of AF + burst pacing (%)	burst pacing time (%)	burst ON (sec)	burst OFF (sec)
1	31	85	83	10	2
2	18	91	91	10	1
3	53	73	71	5	2
4	55	72	71	5	2
5	29	85	83	10	2
6	22	89	86	19	3
7	6	97	91	20	2
8	7	97	95	20	1
9-14	<1	>99	100	10	0

Supplement Figure 1: Explanation of *atrial fibrillation pacing control* (AFPC) group. This group was designed to replicate the total AF and burst pacing stress on the atria in CaMKIIn-expressing animals to eliminate AF/burst pacing burden as a confounder for structural remodeling. The burst pacing burden for all other groups was 50% (2 second on/off cycling). To reproduce the burst pacing/AF burden of the AF control group, the daily percentage of non-burst pacing segments showing AF was added to the baseline burst pacing time of 50% to give a total percentage of time with either AF or burst pacing. The burst on and burst off times in the pacemaker were reprogrammed daily in the AFPC group to reproduce the total AF/burst pacing time measured in the AF-control group.

Supplement Figure 2

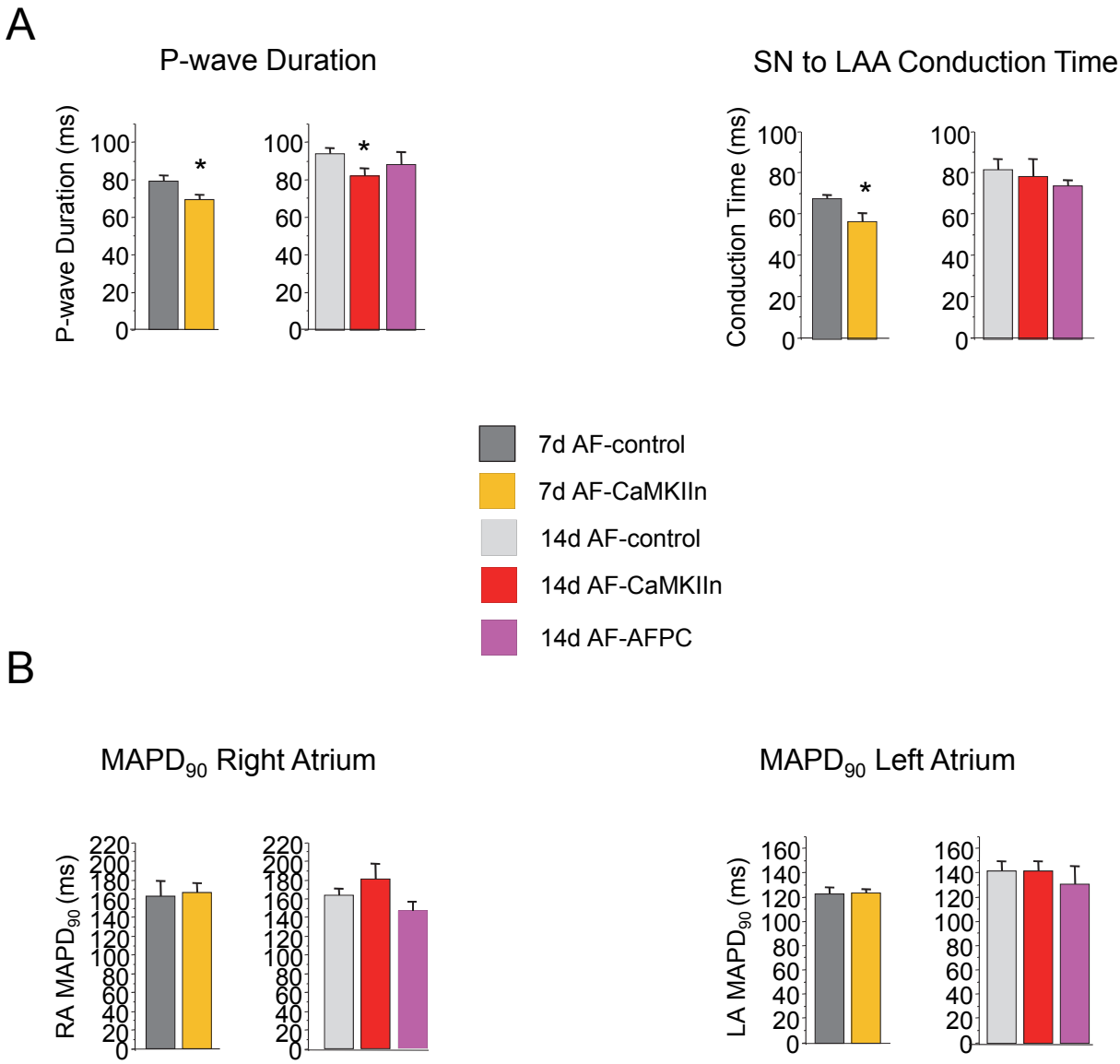

Supplement Figure 2: Electrophysiological data from sacrifice study: **(A)** P-wave duration during sinus rhythm and intra-atrial conduction time during pacing at the sinus node (SN) and recording at the tip of the left atrial appendage (LAA), and **(B)** monophasic action potential duration to 90% repolarization ($MAPD_{90}$). Atrial $MAPD_{90}$ measurements are the average of 5 measurements per chamber per animal. * $p<0.05$ compared to control.

Supplemental Figure 3

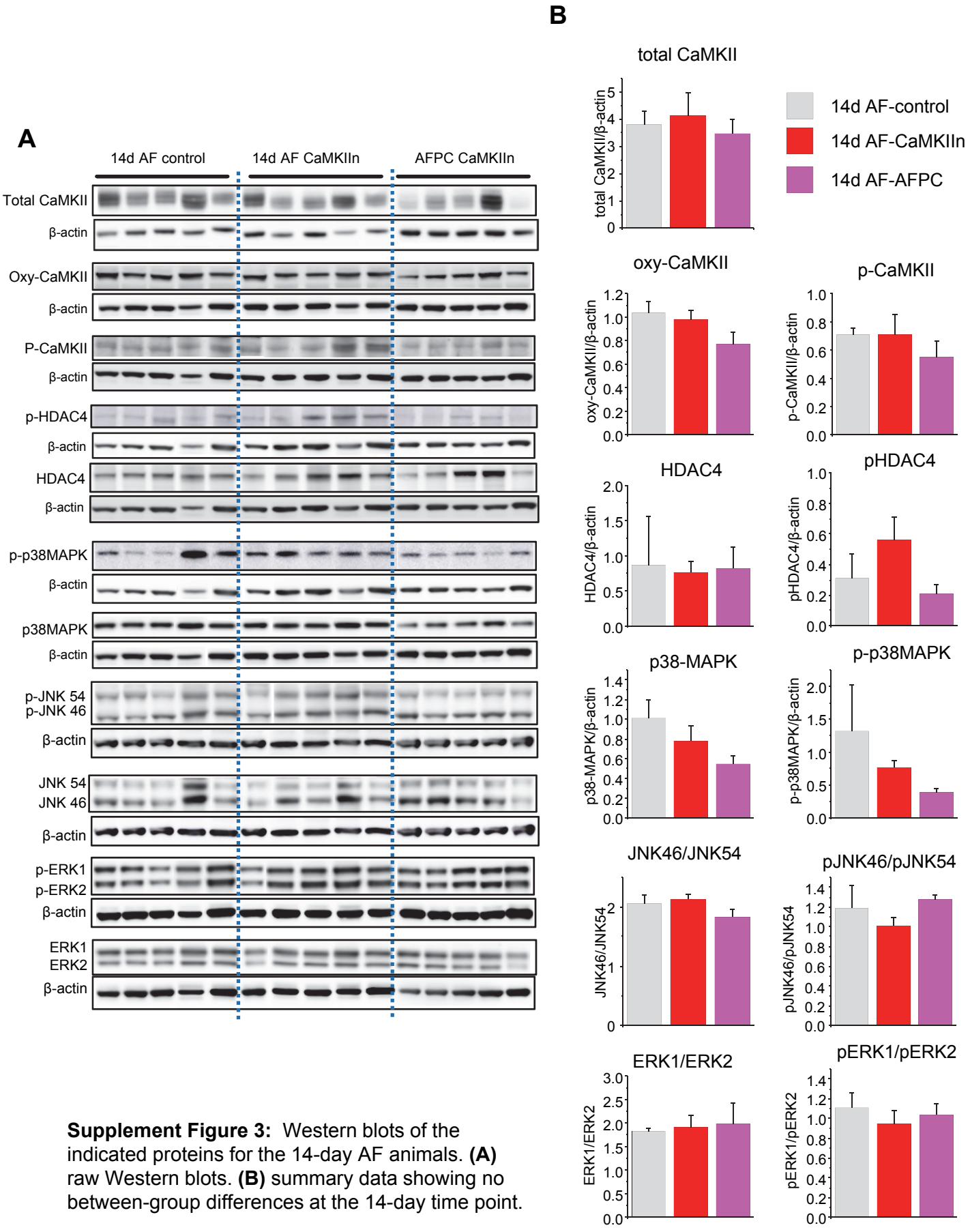

Supplement Figure 3: Western blots of the indicated proteins for the 14-day AF animals. **(A)** raw Western blots. **(B)** summary data showing no between-group differences at the 14-day time point.

Supplement Figure 4

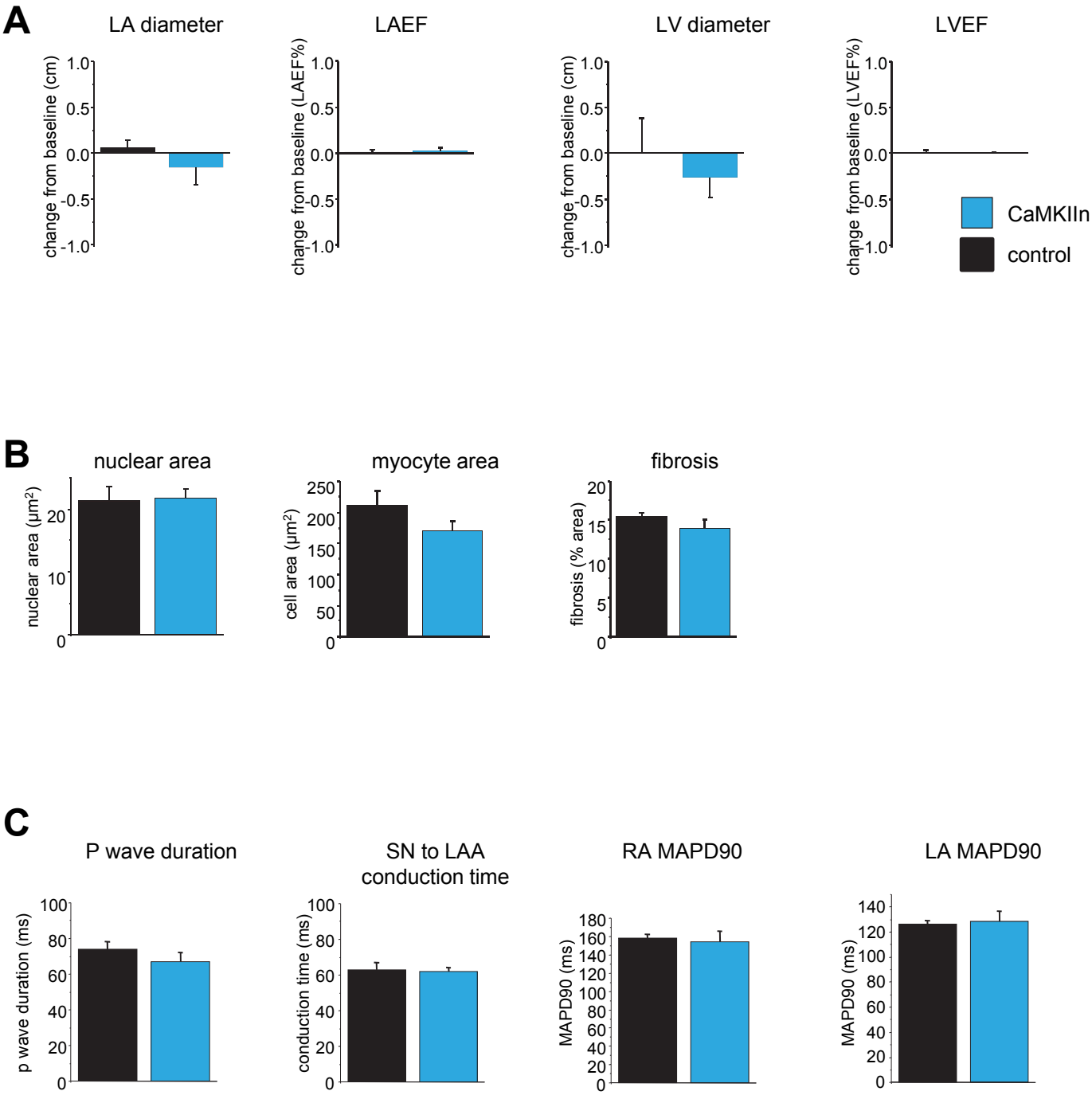

Supplement Figure 4: Sinus rhythm animals. **(A)** Echocardiographic measures of left atrial (LA) end-diastolic diameter and ejection fraction (LAEF) and left ventricular (LV) end-diastolic diameter and ejection fraction (LVEF) were not different between groups. **(B)** histology measures of nuclear and cell area and fibrosis were not different between groups. **(C)** Electrophysiological measures of atrial conduction and repolarization did not differ between groups. **(D)** Protein expression for various proteins in the CaMKII signaling pathways also did not differ between groups.

Supplement Figure 5

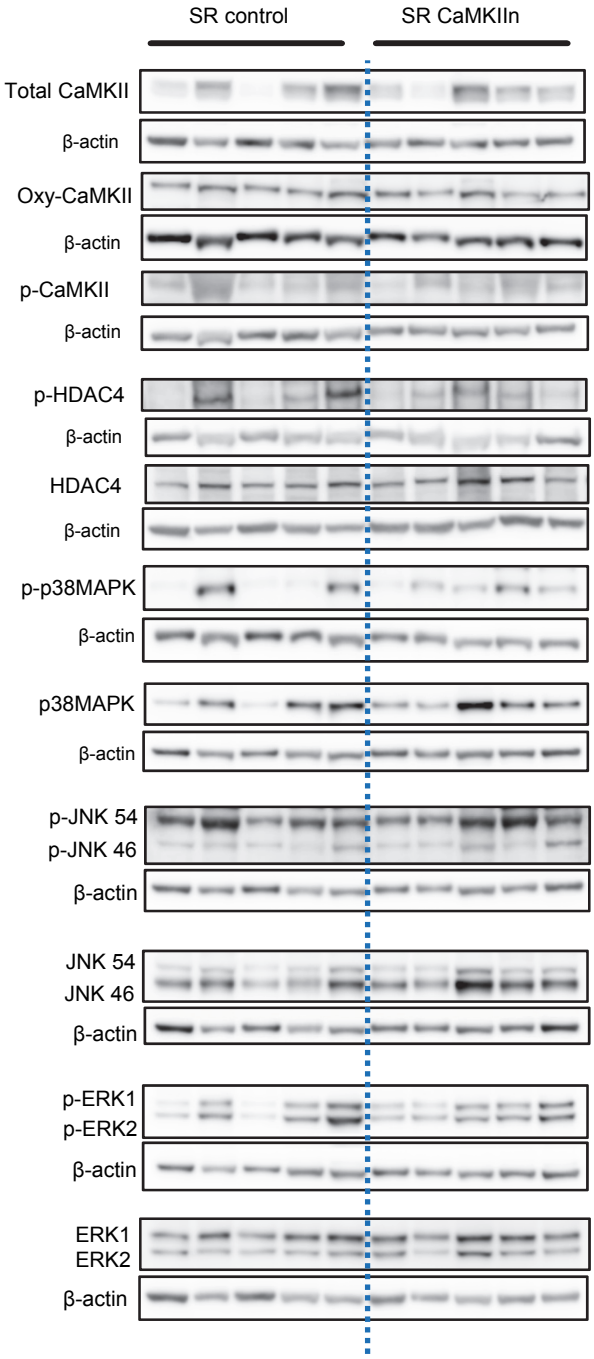

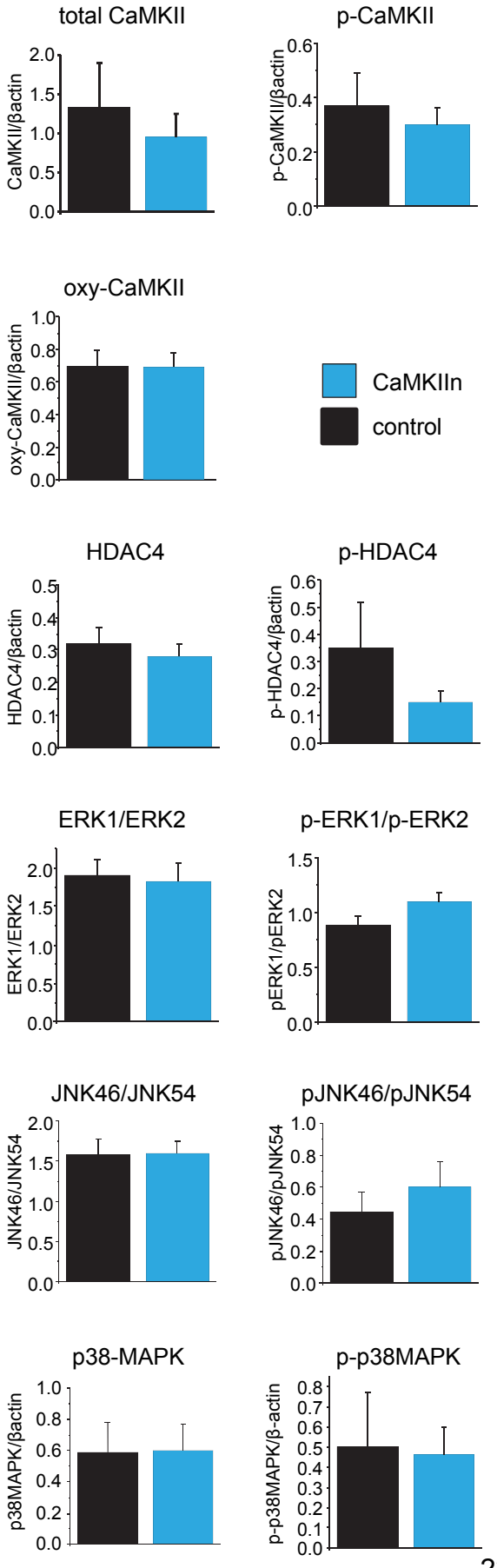

Supplement Figure 5: Western blots of the indicated proteins for the 7-day SR animals. Normalization was to the within-blot β-actin band shown for each blot.

Supplement Figure 6

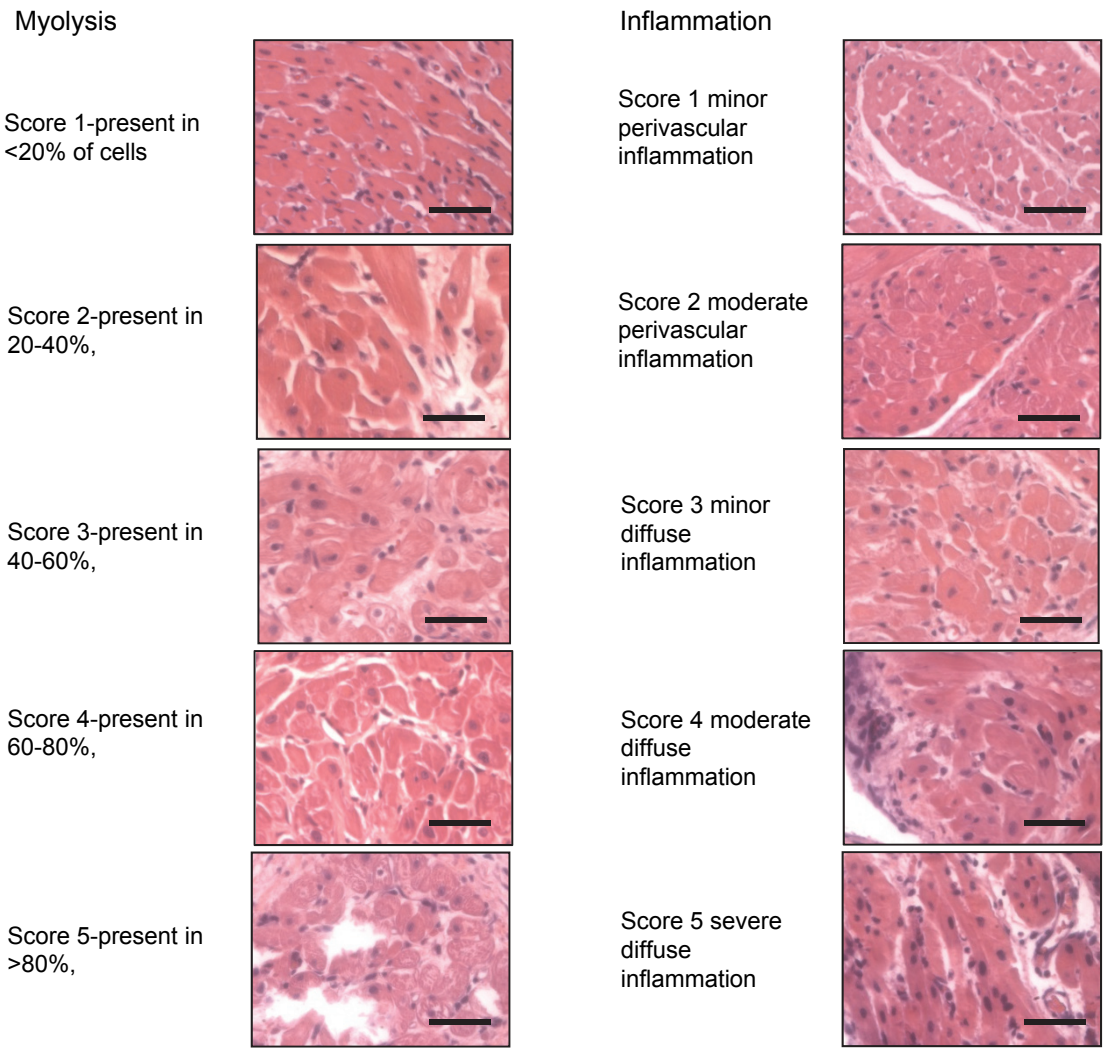

Supplement Figure 6: examples and descriptions used for assigning myolysis and inflammation grades to the histology samples.

Supplement Figure 7

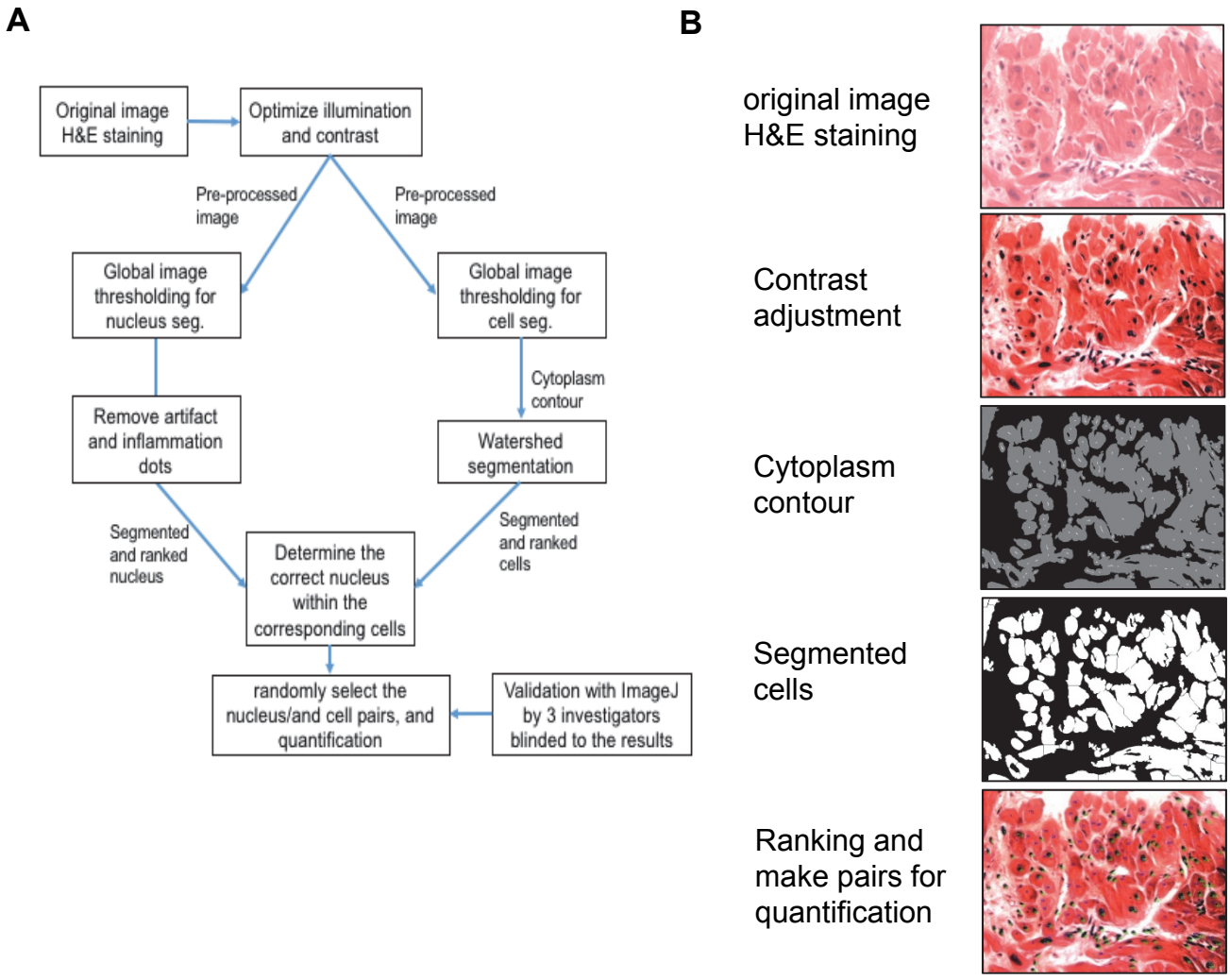

Supplement Figure 7: schematic illustrating the image processing steps used to measure cell and nuclear sizes.

Supplement Figure 8

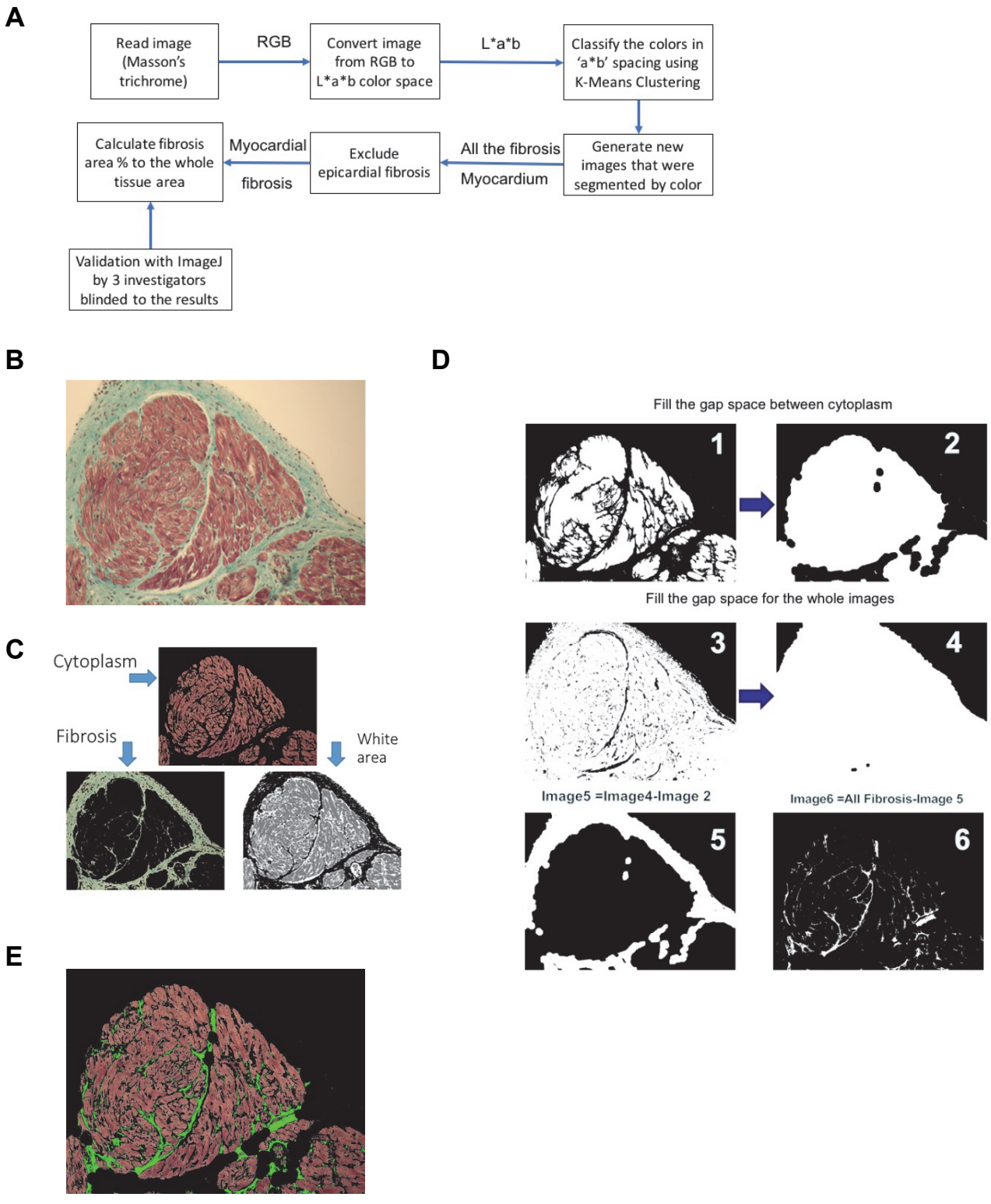

Supplement Figure 8: schematic showing the processing to quantify fibrosis.